

## Corrosion Inhibition Effect of N-lauroyl L-lysine on Mild Steel in 0.5 M H<sub>2</sub>SO<sub>4</sub> Solution

Xianguang Zeng<sup>1,2</sup>, Lin Zhu<sup>3,\*</sup> and Xingwen Zheng<sup>2,3,\*</sup>

<sup>1</sup> School of Materials Science and Engineering, Sichuan University of Science & Engineering, Zigong 643000, China

<sup>2</sup> Key Laboratory of Material Corrosion and Protection of Sichuan Province, Zigong 643000, China

<sup>3</sup> School of Chemical and Environmental Engineering, Sichuan University of Science & Engineering, Zigong 643000, China

\*E-mail: [adinchem@126.com](mailto:adinchem@126.com), [zxwasd@126.com](mailto:zxwasd@126.com)

*Received:* 5 February 2020 / *Accepted:* 26 March 2020 / *Published:* 10 May 2020

---

The inhibitive effect of N-lauroyl L-lysine on the corrosion of mild steel in 0.5 M H<sub>2</sub>SO<sub>4</sub> solution was investigated by electrochemical technique, weight loss measurement, scanning electron microscope (SEM) and quantum chemical calculation. The results showed that N-lauroyl L-lysine was a moderate cathodic inhibitor for mild steel in 0.5 M H<sub>2</sub>SO<sub>4</sub> solution with its inhibition efficiency increasing with concentration, and decreasing with temperature. The adsorption of N-lauroyl L-lysine on the surface of mild steel obeyed El-Awady thermodynamic-kinetic model, and the thermodynamic and kinetic parameters, as well as quantum chemical parameters, were determined to discuss the mechanism of inhibition of N-lauroyl L-lysine on mild steel surface.

---

**Keywords:** N-lauroyl L-lysine, mild steel, corrosion inhibitor, adsorption, quantum chemical calculation

### 1. INTRODUCTION

Corrosion inhibitors, as additives, which can effectively inhibit the corrosion of metals in acid medium, have been widely used in many industrial fields [1-3]. With the improvements of environmental protection awareness and the requirements for sustainable development, developing environmentally friendly corrosion inhibitors has become a growing demand. Amino acids contain amino and carboxyl groups, which are considered as active groups of corrosion inhibitors, and due to their ease of production, low price, non toxicity and easy degradation, the inhibition performance of amino acids is an attractive research interest. Mobin et al. [4] found that L-cysteine significantly reduced the corrosion rate of mild steel in 1 M HCl solution, and the inhibition efficiency was

noticeably increased in the presence of surfactants, including sodium dodecyl sulphate, cetyl pyridinium chloride and triton X-100. Mendonça and co-workers [5] reported the inhibitory effect of six amino acids on the corrosion of carbon steel and copper in 0.5 mol/L H<sub>2</sub>SO<sub>4</sub> solution, and the results showed that the order of inhibition efficiency of the amino acids on steel and copper were different, and there was a good linear correlation between the inhibition efficiency and the interaction energy calculated by Monte Carlo method considering the presence of water molecules. Similar studies had also been reported by Kaya et al. [6], where they investigated the corrosion inhibition performance of amino acids using quantum chemical calculations and molecular dynamic simulation employing Monte Carlo sampling approach, the theoretical results was in agreement with experimental data, and their results suggested that arginine was a good corrosion inhibitor. Our previous study showed the corrosion inhibition performance of L-lysine as well as its synergism with chloride on mild steel surface in acidic solutions [7]. In the present work, a derivative of L-lysine, N-lauroyl L-lysine, consisting of a long carbon chain introduced into L-lysine to improve its corrosion inhibition performance, is investigated as corrosion inhibitor of mild steel in 0.5 M H<sub>2</sub>SO<sub>4</sub> by electrochemical techniques and gravimetry, and its inhibitive mechanism and performance are analyzed by quantum chemical calculations.

## 2. EXPERIMENTAL

### 2.1. Materials

N-lauroyl L-lysine was purchased from Aladdin Reagent (Shanghai) Co., Ltd. The steel used was Q235 steel sheet. The experimental samples were processed by wire-electrode cutting, and then grinded by SiC abrasive paper (grade 200~800), rinsed with deionized water, degreased by acetone and air-dried. The corrosive medium (0.5 M H<sub>2</sub>SO<sub>4</sub> solution) was prepared by diluting analytical grade sulphuric acid in deionized water.

### 2.2. Electrochemical measurements

Electrochemical experiments were conducted at 298 K in a three-electrode system using CHI660E electrochemical workstation (Shanghai Chenhua Instrument Co. Ltd.). A steel sample with exposed area of 0.785 cm<sup>2</sup> was used as working electrode, while the counter electrode and reference electrode was platinum electrode and saturated calomel electrode (SCE), respectively. First, the open circuit potential (OCP) of mild steel in the test solution was monitored for 30 minutes, followed by the electrochemical impedance spectroscopy (EIS) which was measured at OCP using AC signal with an amplitude of 5 mV in the frequency range from 10<sup>-2</sup> Hz to 10<sup>5</sup> Hz, and then the potentiodynamic polarization was conducted in the potential range of -250 to +250 mV versus OCP with 0.5 mV/s scan rate.

### 2.3. Weight loss measurement and morphology analysis

The dimension of steel sample for weight loss experiment was 50 mm × 25 mm × 5 mm, while that for morphology analysis was 15mm × 10mm × 5mm. The dried samples were accurately weighed and immersed in 500 mL of 0.5 M H<sub>2</sub>SO<sub>4</sub> solution without and with 0.5 mM N-lauroyl L-lysine for 4 h at different temperatures (298 K, 308 K and 318 K). After that the test duration, the samples were taken out and rinsed with water. The corrosion products were removed with an eraser, and the samples were successively cleaned ultrasonically in ethanol and acetone, then dried and reweighed. The corrosion rate ( $v$ ) and the inhibition efficiency ( $\eta$ ) were calculated as follows:

$$v = (m_1 - m_2)/(S \times t) \quad (1)$$

$$\eta = (1 - v_{inh}/v_0) \times 100 \% \quad (2)$$

where  $m_1$  and  $m_2$  are the weights of the sample before and after the test,  $S$  is the surface area of the steel sample,  $t$  is the experimental time, and  $v_{inh}$  and  $v_0$  are the corrosion rates of mild steel in the inhibited solution and in blank solution, respectively. The surface morphologies of the samples after immersion were examined by scanning electron microscope (SEM) using Tescan Vega3 SEM instrument at high vacuum.

### 2.4. Quantum Chemical Calculations

The molecular structure of N-lauroyl L-lysine was geometrically optimized and the related quantum chemical parameters were conducted through Gaussian G09 program using the B3LYP method of density functional theory (DFT) at the basis set level of 6-311++G(d, p).

## 3. RESULTS AND DISCUSSION

### 3.1. OCP-time curves

Figure 1 shows the OCP-time curves of mild steel samples in 0.5 M H<sub>2</sub>SO<sub>4</sub> solutions without and with different concentrations of N-lauroyl L-lysine at 298K. It can be seen that the OCP first increased with time and then became stable around 1200s. It is also noted that the higher the inhibitor concentration, the earlier the OCP stabilized, and its value is more positive, which reflects the inhibition of N-lauroyl L-lysine on mild steel corrosion.

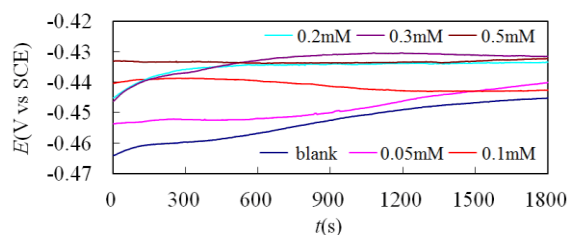


**Figure 1.** OCP-time curves of mild steel samples in 0.5 M H<sub>2</sub>SO<sub>4</sub> solutions without and with different concentrations of N-lauroyl L-lysine at 298K.

### 3.2. Potentiodynamic polarization curves

Potentiodynamic polarization curves of mild steel in 0.5 M H<sub>2</sub>SO<sub>4</sub> solutions without and with different concentrations of N-lauroyl L-lysine at 298 K are presented in Figure 2. From the figure, it is evident that after adding the corrosion inhibitor, the anodic branches of the polarization curves were only slightly affected and almost overlapped, while the cathodic branches of the curves shifted to the direction of low current density with increase in inhibitor concentration, and the cathodic polarization curves appeared parallel to each other, indicating that N-lauroyl L-lysine mainly impeded the cathodic reaction of mild steel in 0.5 M H<sub>2</sub>SO<sub>4</sub> solution, but the corrosion mechanism of mild steel did not show any change in the presence of the inhibitor, implying that N-lauroyl L-lysine inhibited the corrosion process only by adsorbing or blocking the surface active sites present on the steel surface [8-10].

Because there are no obvious linear Tafel regions in the anodic polarization curves, the corrosion electrochemical parameters are obtained by Tafel extrapolation method from the cathodic polarization curves [11], and the data are listed in Table 1, where  $E_{\text{corr}}$  and  $I_{\text{corr}}$  respectively represent corrosion potential and corrosion current density,  $\beta_c$  is the cathodic Tafel slope, and inhibition efficiency ( $\eta$ ) is calculated by the following equation:

$$\eta = \left(1 - \frac{I_{\text{corr,inh}}}{I_{\text{corr,0}}}\right) \times 100\% \quad (3)$$

where  $I_{\text{corr,inh}}$  and  $I_{\text{corr,0}}$  are the corrosion current densities of mild steel in the presence and absence of the inhibitor, respectively.

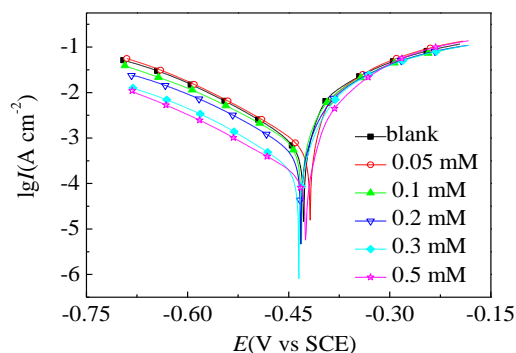


**Figure 2.** Potentiodynamic polarization curves of mild steel in 0.5 M H<sub>2</sub>SO<sub>4</sub> solutions without and with different concentrations of N-lauroyl L-lysine at 298 K.

Table 1 shows that with the increase in N-lauroyl L-lysine concentration, the value of  $I_{\text{corr}}$  decreased and the inhibition efficiency increased. The inhibition efficiency reached 85.1 % at 0.5 mM. The corrosion potential did not change significantly with the addition of the inhibitor. This means that the presence of N-lauroyl L-lysine had little effect on the mechanism of hydrogen evolution reaction. It is generally believed that only when the magnitude of  $E_{\text{corr}}$  shift is greater than 85mV, that the inhibitor can be regarded as anode-type or cathode-type, otherwise it is mixed-type [12-14]. It can be observed from Table 1 that the shift in  $E_{\text{corr}}$  is less than 20 mV, but according to Figure 2, N-lauroyl L-lysine has weak inhibitive effect on the anodic reaction, whereas it obviously inhibits the cathodic reaction. Therefore, N-lauroyl L-lysine should be considered as a moderate cathodic inhibitor for mild steel in

0.5 M H<sub>2</sub>SO<sub>4</sub> solution.

**Table 1.** Corrosion electrochemical parameters for mild steel in 0.5 M H<sub>2</sub>SO<sub>4</sub> solution without and with different concentrations of N-lauroyl L-lysine at 298 K.

<i>c</i> (mM)	<i>E</i> <sub>corr</sub> (V vs SCE)	-β <sub>c</sub> (mV/dec)	<i>I</i> <sub>corr</sub> (mA·cm <sup>-2</sup> )	η(%)
blank	-0.428	136	0.891	\
0.05	-0.418	134	0.789	11.5
0.1	-0.431	125	0.649	27.2
0.2	-0.432	125	0.493	44.7
0.3	-0.435	114	0.199	77.7
0.5	-0.425	121	0.132	85.1

### 3.3. EIS

Figure 3 shows the Nyquist plots and Bode plots for mild steel in 0.5 M H<sub>2</sub>SO<sub>4</sub> in the absence and presence of various concentrations of N-lauroyl L-lysine at 298 K. It is clear that after adding N-lauroyl L-lysine, the shape of the impedance spectrum did not change significantly except for the increase of impedance, indicating that the N-lauroyl L-lysine had little effect on the corrosion reaction mechanism of mild steel in 0.5 M H<sub>2</sub>SO<sub>4</sub> [15]. The Nyquist diagram is composed of a capacitive loops at high frequency and small inductive loops at low frequency, and due to the frequency dispersion of the interfacial impedance and the inhomogeneous electrode surface caused by the microscopic roughness and inhibitor adsorption, the Nyquist plots show depressed semicircles [16]. Meanwhile, combined with the features of Bode plots, the impedance parameters are obtained by fitting EIS to the equivalent circuit as shown in Figure 4 using ZSimpWin software [17], the results are given in Figure 5. In the circuit, *R*<sub>s</sub> is the resistance of solution, *L* and *R*<sub>L</sub> represent the inductive impedance and inductive resistance, respectively, and *R*<sub>ct</sub> is the charge transfer resistance. Constant phase element (CPE) is usually used to replace capacitance (*C*) to provide a more accurate fitting [18]. The inhibition efficiency (η) is calculated using charge transfer resistance by the following equation:

$$\eta = (1 - R_{ct,0}/R_{ct,inh}) \times 100 \% \quad (4)$$

where *R*<sub>ct,inh</sub> and *R*<sub>ct,0</sub> are charge transfer resistances in the presence and absence of inhibitor, respectively.

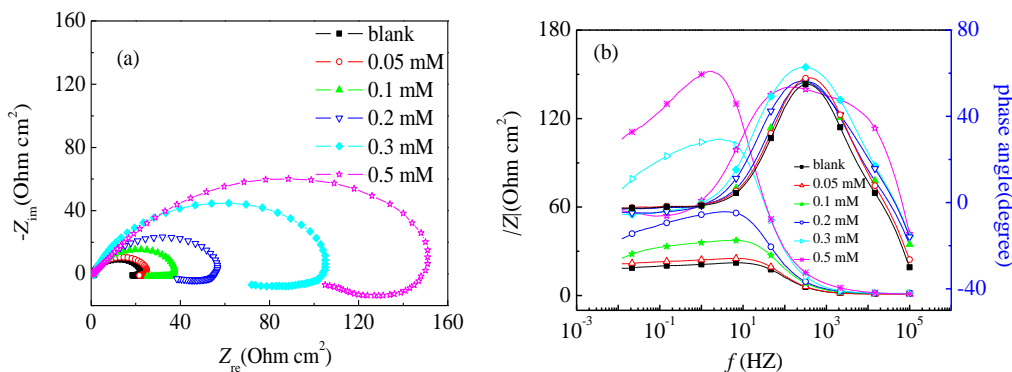


**Figure 3.** Nyquist plots (a) and Bode plots (b) for mild steel in 0.5 M H<sub>2</sub>SO<sub>4</sub> solution without and with different concentrations of N-lauroyl L-lysine at 298 K.

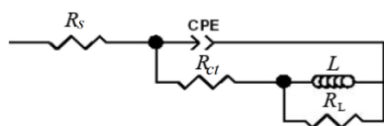


**Figure 4.** Equivalent circuit applied for fitting the impedance spectra.

As shown in Figure 5, the values of  $R_{ct}$  increased with increase in N-lauroyl L-lysine concentration, and the increase is attributed to the adsorption of N-lauroyl L-lysine molecule on the mild steel/solution interface leading to the formation of a protective layer on the electrode surface to control the extent of mild steel dissolution [19, 20]. The inhibition efficiency increased with the concentration of the inhibitor, and it is consistent with the results of potentiodynamic polarization measurements.

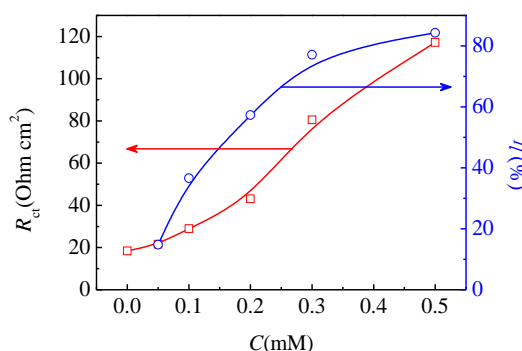


**Figure 5.** The values of  $R_{ct}$  and  $\eta$  obtained from EIS for mild steel in 0.5 M H<sub>2</sub>SO<sub>4</sub> solution without and with different concentrations of N-lauroyl L-lysine at 298 K.

### 3.4. Weight loss measurements and morphology analysis

In order to further confirm the inhibition performance of N-lauroyl L-lysine, the corrosion rates

of mild steel in 0.5 M H<sub>2</sub>SO<sub>4</sub> solution without and with 0.5 mM N-lauroyl L-lysine were evaluated by weight loss method. Correspondingly, the corrosion inhibition efficiency is calculated, and the results are listed in Table 2. The table reveals that N-lauroyl L-lysine can effectively inhibit the corrosion of mild steel in 0.5 M H<sub>2</sub>SO<sub>4</sub> solution. The inhibition performance of the inhibitor is also confirmed by the corrosion morphology of the steel sample surface after immersion in 0.5 M H<sub>2</sub>SO<sub>4</sub> solution without and with 0.5 mM N-lauroyl L-lysine at 298 K for 4 h. This is presented in Figure 6. Moreover, it is also observed from Table 2 that as the dissolution rate of steel increased with increase in temperature, the stripping effect of the corrosion inhibitor was enhanced, making it difficult to adsorb on the surface of mild steel, thereby leading to decreased inhibition efficiency.

**Table 2.** Corrosion rate and inhibition efficiency obtained by weight loss measurement.

c(mM)	25°C		35°C		45°C	
	v(g·m <sup>2</sup> ·h <sup>-1</sup> )	η(%)	v(g·m <sup>2</sup> ·h <sup>-1</sup> )	η(%)	v(g·m <sup>2</sup> ·h <sup>-1</sup> )	η(%)
blank	18.1	/	33.8	/	46.2	/
0.5	3.5	80.7	7.3	78.4	17.4	62.3

### 3.5. Thermodynamic and kinetic analysis

Corrosion inhibitors are generally considered to play roles in corrosion inhibition by adsorption, and adsorption isotherm equations are often employed to describe the adsorption behavior of corrosion inhibitors, which is the relationship between concentration and surface coverage ( $\theta$ ), and the value of  $\theta$  is calculated from the inhibition efficiency, that is,  $\theta = \eta/100$ . Using inhibition efficiency data obtained from polarization and EIS measurements, the relationship between the surface coverage and concentration in this study is found to be in accordance with El-Awady thermodynamic-kinetic model (equation 5) [21,22], and the fitting results are shown in Figure 7.

$$\ln \frac{\theta}{1-\theta} = y \ln C + \ln K' \quad (5)$$

where,  $y$  is the number of inhibitor molecules adsorbed on one active site, the adsorption equilibrium constant  $K_{\text{ads}}$  is calculated by the following equation [21,22]:

$$K_{\text{ads}} = K'^{(1/y)} \quad (6)$$

The values of  $y$  and  $K_{\text{ads}}$  are calculated by the fitting the slopes and intercepts, and the results are shown in Table 3. The value of  $y$  is greater than one, signifying the formation of multilayers of N-lauroyl L-lysine on the steel surface [21]. The high value of  $K_{\text{ads}}$  is associated with strong adsorption of the inhibitor on the surface of the mild steel in 0.5 M H<sub>2</sub>SO<sub>4</sub> solution, and the adsorption free energy ( $\Delta G_{\text{ads}}$ ) is further calculated as follows [23,24]:

$$K_{\text{ads}} = \frac{1}{55.5} \exp\left(-\frac{\Delta G_{\text{ads}}}{RT}\right) \quad (7)$$

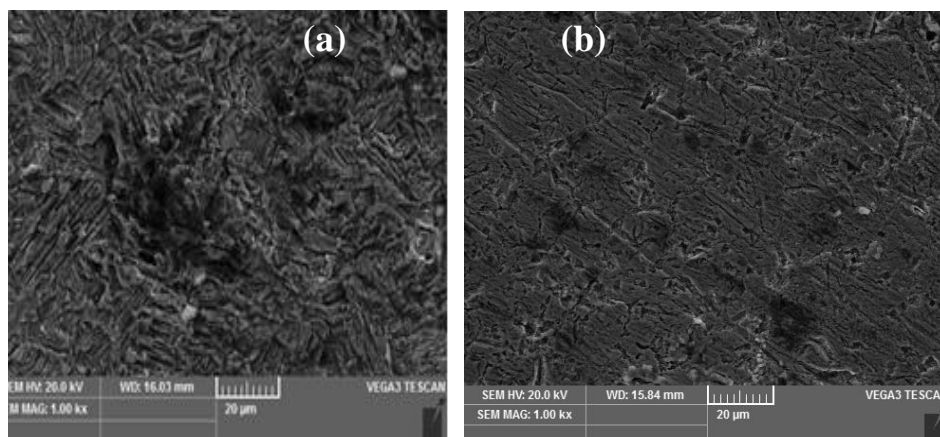


**Figure 6.** SEM images of mild steel sample immersed in 0.5 M H<sub>2</sub>SO<sub>4</sub> solution without and with 0.5 mM N-lauroyl L-lysine at 298 K for 4 h.

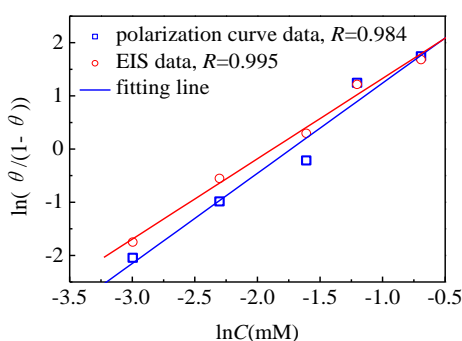


**Figure 7.** Fitting line of El-Awady thermodynamic-kinetic model for the adsorption of N-lauroyl L-lysine on the surface of mild steel in 0.5 M H<sub>2</sub>SO<sub>4</sub> at 298 K.

The data in Table 3 shows that the fitting results of the polarization curves and EIS spectra are in good agreement, the value of  $\Delta G_{ads}$  is between -20 and -40 kJ/mol, which means that the adsorption of N-lauroyl L-lysine on the surface of mild steel is a spontaneous process, and the adsorption involves both physical adsorption and chemical adsorption [24].

**Table 3.** Adsorption parameters of N-lauroyl L-lysine on the surface of mild steel in 0.5M H<sub>2</sub>SO<sub>4</sub> at 298K.

Polarization curve			EIS		
y	$K_{ads}(L\ mol^{-1})$	$\Delta G_{ads}(kJ\ mol^{-1})$	1/y	$K_{ads}(L\ mol^{-1})$	$\Delta G_{ads}(kJ\ mol^{-1})$
1.70	6545	-29.1	1.51	5648	-28.7

Temperature is an important factor affecting the performances of corrosion inhibitors, the related activation parameters of the corrosion process of mild steel in 0.5 M H<sub>2</sub>SO<sub>4</sub> solution without and with 0.5 mM N-lauroyl L-lysine are obtained by fitting the data in Table 3 through Arrhenius equation [25, 26]. The fitted lines are shown in Figure 8, and the calculated activation parameters are

given in Table 4.

$$\ln v = -\frac{E_a}{RT} + \ln \lambda \tag{8}$$

where  $v$  is corrosion rate,  $R$  is gas constant,  $T$  is thermodynamic temperature,  $E_a$  is apparent activation energy and  $\lambda$  is pre-exponential factor.

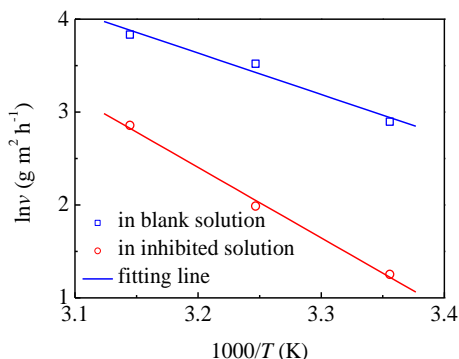
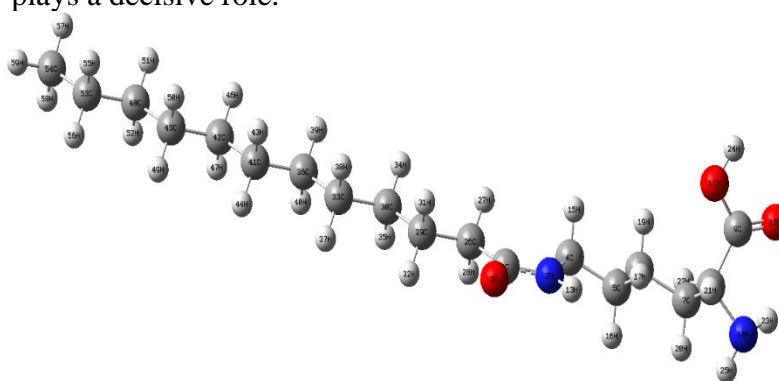


**Figure 8.** Arrhenius plots for mild steel in 0.5 M H<sub>2</sub>SO<sub>4</sub> solution without and with 0.5 mM N-lauroyl L-lysine.

**Table 4.** Activation parameters of mild steel in 0.5 M H<sub>2</sub>SO<sub>4</sub> solution without and with 0.5 mM N-lauroyl L-lysine.

C(mM)	E <sub>a</sub> (kJ/mol)	λ
blank	37.03	5.88×10 <sup>7</sup>
0.5	63.10	3.90×10 <sup>11</sup>

Table 4 shows that the activation energy of the corrosion reaction of mild steel in inhibited solution is greater than that in the blank solution. This is due to the adsorption of inhibitors on the steel surface which impedes its corrosion process. However, the value of pre-exponential factor also increased, which indicates that the corrosion process is not only controlled by activation energy, but the activation energy plays a decisive role.



(a) optimized structure

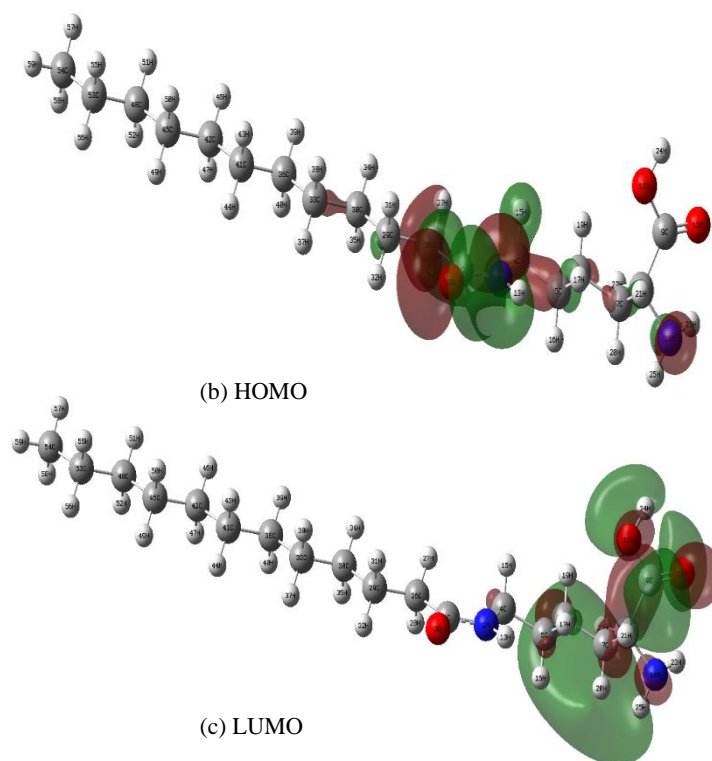


**Figure 9.** Optimized structure and the frontier orbital electron density distribution of N-lauroyl L-lysine.

### 3.6. Quantum chemical study

To further understand the interaction between the inhibitor molecule and mild steel, using the Gaussian 09 software, the optimized structure of N-lauroyl L-lysine and its electron density distribution of the frontier orbitals are shown in Figure 9. According to the frontier molecular orbital theory, the highest occupied molecular orbital (HOMO) and the lowest unoccupied molecular orbital (LUMO) are related to the electron donating ability and the ability to accept electrons, respectively. The electron density of HOMO is mainly distributed on N atom of the terminal group of L-lysine and its bonded carbonyl group, while that of LUMO is mainly concentrated on the  $\alpha$ -N and carboxyl group of lysine, suggesting that heteroatoms of N and O are the active adsorption centers of N-lauroyl L-lysine.

The energy of HOMO ( $E_{\text{HOMO}}$ ), the energy of LUMO ( $E_{\text{LUMO}}$ ), energy gap ( $\Delta E = E_{\text{LUMO}} - E_{\text{HOMO}}$ ) and dipole moment ( $\mu$ ) are calculated and listed in Table 5. In general, a large value of  $E_{\text{HOMO}}$  means that molecule has a strong ability to donate electrons, while a low  $E_{\text{LUMO}}$  value indicates that the ability of accepting electrons is strong [27-29]. The lower the value of  $\Delta E$  is, the more reactive the molecule is, implying a better corrosion inhibition [30-34]. Dipole moment reflects the strength of molecular polarity, and the increase in dipole moment can promote the adsorption process of the inhibitor [7,27]. As comparison, the parameters of L-lysine are also given in Table 5. It can be seen that, with the introduction of lauroyl group,  $E_{\text{LUMO}}$  significantly increased, the value of  $\Delta E$  decreased, and the dipole moment increased, indicating that N-lauroyl L-lysine has stronger inhibitive

performance than L-lysine, and that is consistent with the experimental result.

**Table 5.** Quantum chemistry parameters of N-lauroyl L-lysine and L-lysine

inhibitor molecule	$E_{\text{HOMO}}(\text{eV})$	$E_{\text{LUMO}}(\text{eV})$	$\Delta E(\text{eV})$	$\mu(\text{D})$	$\eta(\%)^1$	reference
N-lauroyl L-lysine	-6.89	-0.85	6.04	4.00	77.7/77.1	this work
L-lysine	-6.70	-0.44	6.26	2.93	28.7/42.9	[7]

**Note:** The inhibition efficiency is the value when the concentration of inhibitor is 0.3 mM, first obtained from polarization curve and then from EIS.

#### 4. CONCLUSIONS

N-lauroyl L-lysine as a moderate cathodic inhibitor mainly suppressed the cathodic reaction of mild steel in 0.5 M  $\text{H}_2\text{SO}_4$  solution, the inhibition efficiency increased with increase in inhibitor concentration but decreased with the increase in temperature. The inhibition efficiency of 0.5 mM N-lauroyl L-lysine was up to 80 % at 298 K. The heteroatoms (N and O) are active adsorption sites of N-lauroyl L-lysine, they can spontaneously adsorb on the surface of mild steel and result in the increase of activation energy and charge transfer resistance of the corrosion reaction process of mild steel in 0.5 M  $\text{H}_2\text{SO}_4$  solution, moreover, the adsorption accords with El-Awady thermodynamic-kinetic model and involved both physical and chemical adsorptions.

#### ACKNOWLEDGEMENTS

This project is supported financially by Talent Project of Sichuan University of Science & Engineering (No. 2016RCL11) and the Opening Project of Key Laboratory of Material Corrosion and Protection of Sichuan Province (No. 2016CL03).

#### References

1. T.F. Souza, M. Magalhães, V.V. Torres and E. D'Elia, *Int. J. Electrochem. Sci.*, 10 (2015) 22.
2. B. Tan, S. Zhang, Y. Qiang, W. Li, H. Li, L. Feng, L. Guo, C. Xu, S. Chen and G. Zhang, *J. Mol. Liq.*, 298 (2020) <https://doi.org/10.1016/j.molliq.2019.111975>.
3. P.M. Krishnegowda, V.T. Venkatesha, P.K.M. Krishnegowda and S.B. Shivayogiraju, *Ind. Eng. Chem. Res.*, 52 (2013), 722.
4. M. Mobin, S. Zehra and M. Parveen, *J. Mol. Liq.*, 216 (2016) 598.
5. G.L.F. Mendonça, S.N. Costa, V.N. Freire, P.N.S. Casciano, A.N. Correia and P.D. Lima-Neto, *Corros. Sci.*, 115 (2017) 41.
6. S. Kaya, B. Tüzün, C. Kaya and I.B. Obot, *J. Taiwan Inst. Chem. E.*, 58 (2016) 528.
7. X. Zheng, M. Gong and C. Liu, *Int. J. Electrochem. Sci.*, 12 (2017) 5553.
8. M. Mobin, S. Zehra and R. Aslama, *RSC Adv.*, 6 (2016) 5890.
9. V. Srivastava, Jiyaul Haque, C. Verma, P. Singh, H. Lgaz, R. Salghi and M.A. Quraishi, *J. Mol. Liq.*, 244 (2017) 340.

10. C. Verma, J. Haque, E.E. Ebenso and M.A. Quraishi, *Results Phys.*, 9 (2018) 100.
11. A. El Bribri, M. Tabyaoui, B. Tabyaoui, H. El Attari and F. Bentiss, *Mater. Chem. and Phys.*, 141 (2013) 240.
12. A. Saxena, D. Prasad, R. Haldhar, G. Singh and A. Kumar, *J. Environ. Chem. Eng.*, 6 (2018) 694.
13. X. Li, S. Deng, T. Lin, X. Xie and G. Du, *J. Taiwan Inst. Chem. E.*, 86 (2018) 252.
14. M. Chevalier, M. Lebrini, F. Robert, S. Sutour, F. Tomi, C. Jama, F. Bentiss and C. Roos, *Int. J. Electrochem. Sci.*, 14 (2019) 1208.
15. A.M. Fathi, H.S. Mandour and A.M.A. Elkarim, *Int. J. Electrochem. Sci.*, 11 (2016) 5580.
16. Y. Qiang, S. Zhang, B. Tan and S. Chen, *Corros. Sci.*, 133 (2018) 6.
17. C. Chai, Y. Xu, S. Shi, X. Zhao, Y. Wu, Y. Xu and L. Zhang, *RSC Adv.*, 8 (2018) 24970.
18. R.F.B. Cordeiro, A.J.S. Belati, D. Perrone and E. D'Elia, *Int. J. Electrochem. Sci.*, 13 (2018) 12188.
19. S.A.E. Wanees, M. Alahmdi, S.M. Rashwan, M.M. Kamel, and M.G.A. Elsadek, *Int. J. Electrochem. Sci.*, 11 (2016) 9265.
20. R. Kumar, O.S. Yadav and G. Singh, *J. Mol. Liq.*, 237 (2017) 413.
21. A.A. El-Awady, B.A. Abd-El-Nabey and S.G. Aziz, *J. Electrochem. Soc.*, 139 (1992) 2149.
22. A.M. Abdel-Gaber, B.A. Abd-El-Nabey and M. Saadawy, *Corros. Sci.*, 51 (2009) 1038.
23. M.A. Albuquerque, M.C.C. de Oliveira and A. Echevarria, *Int. J. Electrochem. Sci.*, 12 (2017) 852.
24. S.A.E. Wanees, M.I. Alahmdi, M.A.E. Azzem and H.E. Ahmed, *Int. J. Electrochem. Sci.*, 11 (2016) 3448.
25. Sudheer and M.A. Quraishi, *Ind. Eng. Chem. Res.*, 53 (2014) 2851.
26. H.K. Sappani and S. Karthikeyan, *Ind. Eng. Chem. Res.*, 53 (2014) 3415.
27. S.K. Saha and P. Banerjee, *RSC Adv.*, 5 (2015) 71120.
28. R.K. Gupta, M. Malviya, C. Verma and M.A. Quraishi, *Mater. Chem. and Phys.*, 198 (2017) 360.
29. T.N.J.I. Edison, R. Atchudan, A. Pugazhendhi, Y.R. Lee and M.G. Sethuraman, *J. Mol. Liq.*, 264 (2018) 483.
30. Y. Zhou, L. Guo, S. Zhang, S. Kaya, X. Luo and B. Xiang, *RSC Adv.*, 7 (2017) 23961.
31. A.S.Fouda, S.M. Abd El-Wahab, M.S. Attia, A.O. Youssef and H.O. Elmoher, *Int. J. Electrochem. Sci.*, 10 (2015) 7866.
32. H. Allal, Y. Belhocine and E. Zouaoui, *J. Mol. Liq.*, 265 (2018) 668.
33. T. He, W. Emori, R.-H. Zhang, P.C. Okafor, M. Yang, C.-R. Cheng, *Bioelectrochem.*, 130 (2019) 107332.
34. W. Emori, R.-H. Zhang, P.C. Okafor, X.-W. Zheng, T. He, W. Kun, X.-Z. Lin, C.-R. Cheng, *Colloids Surf. A Physicochem. Eng. Asp.*, 590 (2020) 124534.